Author Manuscript

Author Manuscript

Author Manuscript

Author Manuscript

HHS Public Access

Author manuscript

Cell. Author manuscript; available in PMC 2014 July 03.

Published in final edited form as:

Cell. 2013 July 3; 154(1): 47–60. doi:10.1016/j.cell.2013.06.007.

Catastrophic nuclear envelope collapse in cancer cell micronuclei

Emily M. Hatch[1], **Andrew H. Fischer**[2], **Thomas J. Deerinck**[3], and **Martin W. Hetzer**[1,*]

[1]Molecular and Cell Biology Laboratory, Salk Institute for Biological Studies, 10010 N. Torrey Pines Road, La Jolla, 92037 CA, USA

[2]Department of Pathology, University of Massachusetts Medical School, 55 Lake Avenue, Worcester, Massachusetts 01655, USA

[3]Department of Neurosciences, National Center for Microscopy and Imaging Research, and Center for Research in Biological Systems, University of California, San Diego, La Jolla, California, 92093-0608, USA

Summary

During mitotic exit missegregated chromosomes can recruit their own nuclear envelope (NE) to form micronuclei (MN). MN have reduced functioning compared to primary nuclei in the same cell, although the two compartments appear to be structurally comparable. Here we show that over 60% of MN undergo an irreversible loss of compartmentalization during interphase due to NE collapse. This disruption of the MN, which is induced by defects in nuclear lamina assembly, drastically reduces nuclear functions and can trigger massive DNA damage. MN disruption is associated with chromatin compaction and invasion of endoplasmic reticulum (ER) tubules into the chromatin. We identified disrupted MN in both major subtypes of human non-small cell lung cancer, suggesting that disrupted MN could be a useful objective biomarker for genomic instability in solid tumors. Our study shows that NE collapse is a key event underlying MN dysfunction and establishes a link between aberrant NE organization and aneuploidy.

Introduction

The nuclear envelope (NE) is comprised of two membranes whose integrity is required for compartmentalization and regulated access of proteins and other macromolecules to the nuclear genome. The NE forms during late anaphase and telophase from association of ER membranes with the chromatin and subsequent fusion of ER sheets (Anderson and Hetzer, 2008a; Lu et al., 2011). NE formation involves sequential recruitment of proteins that establish the major structures of the NE to the decondensing chromatin (Burke and Ellenberg, 2002). These structures include the nuclear pore complexes (NPCs), the nuclear lamina, which is a network of intermediate filament proteins that stabilizes the NE, and

*To whom correspondence should be addressed: hetzer@salk.edu.

Publisher's Disclaimer: This is a PDF file of an unedited manuscript that has been accepted for publication. As a service to our customers we are providing this early version of the manuscript. The manuscript will undergo copyediting, typesetting, and review of the resulting proof before it is published in its final citable form. Please note that during the production process errors may be discovered which could affect the content, and all legal disclaimers that apply to the journal pertain.

Author Manuscript Author Manuscript Author Manuscript Author Manuscript

inner nuclear membrane (INM)-localized proteins, which target the ER to the chromatin and later link the lamina to the membrane (Gant and Wilson, 1997).

Micronuclei (MN) form when a whole or broken chromosome segregates improperly during mitosis and becomes separated from the main chromatin mass. In this study we will focus conceptually on lagging chromosomes, which give rise to MN containing a whole chromosome. During telophase the lagging chromosome recruits its own NE to form a separate compartment from the primary nucleus (PN). During the subsequent mitosis the sequestered DNA can segregate normally or reform a MN (Crasta et al., 2012). Because they are strongly correlated with mitotic errors, MN are regarded as an accurate indicator of genomic instability and aneuploidy (Fenech, 2007).

Previous work on MN in cultured cells identified functional defects in DNA replication, transcription, DNA damage repair, and nuclear protein localization (Hoffelder et al., 2004; Terradas et al., 2009, 2012; Xu et al., 2011; Crasta et al., 2012). Making a MN does not necessarily decrease functionality as DNA replication occurs normally in karyomeres (i.e. MN that form during normal development) during embryogenesis in several species (Lemaitre, 1998). In addition, somatic cells MN appear structurally normal (Paulin-Levasseur et al., 1996; Hoffelder et al., 2004), although nuclear pore protein levels appear to be partially decreased (Hoffelder et al., 2004; Crasta et al., 2012; Terradas et al., 2012).

It is currently unclear whether this broad group of functional defects occurs concurrently or has distinct origins and why it is specific to somatic cell MN. To address these questions, we analyzed the NE in MN in cultured cells and found that the majority of MN irreversibly lose compartmentalization during interphase in both non-transformed and cancer cells, which globally arrests nuclear functioning. We show that MN disruption is the result of changes in lamina organization, but not increased DNA damage, and is followed by invasion of ER membranes into the MN chromatin. We also show that non-small cell lung cancer tumor sections contain disrupted MN, indicating that disrupted MN are a general feature of cancer cells, which could be a useful marker of genomic instability in solid tumors.

Results

Irreversible loss of MN compartmentalization during interphase

To determine why MN have broad dysfunction compared to PN in the same cell, we first examined nuclear compartmentalization of two reporters: 2×RFP fused to a nuclear localization signal (RFP-NLS) and 4×GFP fused to a nuclear export signal (GFP-NES). We performed time-lapse microscopy of U2OS cells and found that, as expected, RFP-NLS accumulated in both the PN and MN compartments in U2OS cells after NE formation whereas GFP-NES was excluded (Figure 1A). However, although the PN maintained proper localization of the reporter proteins throughout interphase, a significant population of MN showed rapid and irreversible loss of RFP-NLS concomitant with a failure to exclude GFP-NES from the chromatin (Figure 1A and Movie S1). Mislocalization of both nuclear and cytoplasmic reporters is indicative of a disrupted nuclear permeability barrier. Thus, we will refer to this event as MN disruption.

Author Manuscript Author Manuscript Author Manuscript Author Manuscript

To determine what proportion of MN undergo disruption, we quantified MN fate by time-lapse imaging of U2OS cells expressing 3×GFP fused to the NLS-containing importin-β binding domain (IBB) and H2B-mCherry. We found that during a single interphase over 65% of the total MN observed became disrupted and only a small percentage were able to repair the NE and re-accumulate GFP-IBB prior to mitosis (Figure 1B). From these experiments we were also able to determine the fate of the MN chromatin after mitosis. We found that disruption had no significant effect on the frequency with which a MN was generated after the second mitosis and that disrupted MN rejoined the PN chromatin at least 50% of the time (Figure 1C).

To confirm that MN disruption involves a complete loss of compartmentalization we first asked whether the endogenous nuclear proteins retinoblastoma (Rb), a cell cycle regulator, and LSD-1, a histone demethylase, were also lost from disrupted MN. We found that LSD-1 and Rb labeling of MN was strongly correlated with the presence of the NLS-reporter and that these proteins were rarely present in disrupted MN (Figure 1D). Thus, the mislocalization of these proteins is a reliable indicator of MN disruption.

Second, we asked whether disrupted MN can actively accumulate nuclear proteins by expressing a shuttling construct containing both an NLS and an NES fused to tdTomato (NES-tdTom-NLS) in U2OS cells and blocking nuclear export. NES-tdTom-NLS accumulated in both the PN and intact MN, but not in the disrupted MN (Figure S1A and S1B), verifying that accumulation of nuclear proteins is abrogated. These data confirm that disrupted MN have completely lost compartmentalization.

We next analyzed MN disruption in cancer lines from different tissues and found a similar proportion of intact and disrupted MN as in U2OS cells (Figure 1E). We then assessed MN disruption in two non-transformed cell lines – the immortalized epithelial cell line RPE-1 stably expressing GFP-NLS (Figure S1C) and the primary fibroblast cell line IMR90. MN integrity in IMR90 cells was determined by LSD-1 labeling. Because these cells normally produce very few MN, we treated cells with nocodazole to induce missegregation of whole chromosomes (Cimini et al., 2001). This treatment also causes a p53 dependent G1 arrest (Li et al., 2010; Thompson and Compton, 2011; Crasta et al., 2012). In both cell lines we found that around 50% of the MN were disrupted 24 h after mitosis (Figure 1F), indicating that MN disruption occurs frequently in both normal and transformed cells.

Next, we asked whether MN disruption was cell cycle specific. First, cells were synchronized by mitotic shake-off after a brief incubation in nocodazole and pulse labeled with EdU to identify S-phase cells prior to fixation at the indicated time points. After mitotic exit almost all MN were intact by time-lapse imaging, however the proportion of intact MN decreased steadily throughout interphase (Figure 1G). Consistent with stochastic MN disruption, time-lapse imaging experiments revealed that MN disruption occurred throughout interphase such that over 50% of MN were disrupted for over half the duration of interphase (Figure S1D).

To determine whether there are cell cycle specific differences in MN disruption frequency, we first synchronized U2OS cells by mitotic shake-off and incubated them up to 48 h in

Author Manuscript Author Manuscript Author Manuscript Author Manuscript

either hydroxyurea (HU) or the Cdk1 inhibitor RO-3306 to arrest them in S or G2 phase, respectively. The concentration of drug used was sufficient to induce arrest, as assessed by FACS analysis (data not shown). Examination of cells fixed over the course of the arrest showed a gradual decrease in the proportion of intact MN in both S and G2 phase arrests (Figure S1E). We also analyzed MN in G1 arrested RPE-1 GFP-NLS cells and found that the proportion of intact MN also decreases during G1 arrest (Figure S1F). These data confirm that MN disruption frequency is cell cycle independent and that the proportion of disrupted MN increases as interphase is extended.

Finally, we asked whether general characteristics of the chromatin in the MN impacted its fate. Using the initial size of the MN as a proxy for chromatin amount, we observed no correlation between MN disruption and chromatin amount (Figure S1G). We also found no difference in disruption frequency in MN that had a centromere (whole-chromosome origin) or in MN that lacked a centromere (broken chromosome origin) (Figure S1H and S1I). These data indicate that the amount of chromatin and presence of a centromere are not significant factors in MN fate.

MN disruption is caused by NE collapse

Because most MN are intact at mitotic exit, we wanted to investigate why they lose compartmentalization as they proceed through interphase. We first asked whether the loss of compartmentalization in disrupted MN was the result of NPC loss. We examined the levels of NPC components in intact and disrupted MN by immunofluorescence and found that the core nucleoporins recognized by mAb414 are present at similar levels in both disrupted and intact MN (Figure S2A and S2B), suggesting that a loss of NPC proteins is not driving compartmentalization loss. The mAB414 labeling did appear to be disorganized in some disrupted MN, however. In contrast, we found that levels of the basket nucleoporins Nup153 and TPR were reduced in disrupted MN (Figure S2C and S2D). However, the loss of TPR and Nup153 is not sufficient to explain the observed defects in nuclear trafficking (Frosst et al., 2002; Mackay et al., 2009).

Second, we asked whether MN disruption is the result of non-mitotic breakdown of the nuclear membrane. We monitored the dynamics of MN disruption by time-lapse imaging of U2OS cells and compared them to the dynamics of interphase NE rupturing in PN, which have been previously characterized (Vargas et al., 2012). We found that the half-time of GFP-IBB loss during MN disruption was similar to that of PN NE rupturing (Figure 2A and 2B and Movies S2 and S3), suggesting that MN lose compartmentalization via disruption of the NE. To distinguish the two processes we will refer to them as “NE rupturing” in the PN and “NE collapse” in the MN.

NE ruptures in the PN are repaired in minutes, yet NE collapse in the MN is almost always irreversible. To investigate alterations in NE structure during MN disruption, we performed time-lapse imaging of cells expressing Sec61B fused to GFP (Sec61B-GFP), which localizes to both the ER and outer nuclear membranes, identified by calreticulin labeling (Figure 2C). We observed that the majority of MN (27/29) underwent an irreversible collapse of both the NE and the chromatin after disruption (Figure S2E and Movie S4). Analysis of fixed cells indicated that loss of Sec61B-GFP from the nuclear rim strongly correlated with MN

Author Manuscript Author Manuscript Author Manuscript Author Manuscript

disruption (Figure 2C and 2D). Unexpectedly, we noticed that Sec61B-GFP was enriched on the exposed MN chromatin. This is unlikely to mark aggregation of ER membranes, as calreticulin does not show a similar aggregation (Figure 2C). Similar results were observed with Sec61B-V5 (Figure S2F) and the INM proteins LBR and Lap2β (data not shown). These results indicate a significant change in the protein composition of chromatin-associated NE/ER membranes after disruption in MN.

We also observed that ER membranes failed to be properly excluded from the chromatin in disrupted MN. To determine if these membranes represented ER tubules, we observed the localization of a tubular ER marker, reticulon 3 (Rtn3) (Voeltz et al., 2006), which is normally excluded from the NE and ER sheets (Anderson and Hetzer, 2007). V5-tagged Rtn3 is depleted from both PN and intact MN NEs, which are labeled by calreticulin (Figure 2E top). However, V5-Rtn3, as well as calreticulin, was present throughout the chromatin in disrupted MN (Figure 2E bottom), indicating an aberrant association of tubular ER with the exposed chromatin. To confirm the invasion of ER into disrupted MN chromatin, we examined MN ultrastructure by transmission electron microscopy (TEM) in U2OS cells fixed either 8 h or 18 h post mitosis. In the 8 h sample, the PN and the MN were both surrounded by an intact NE (Figure 2F, left). However, at 18 h we observed disrupted MN where convoluted, ribosome-studded ER membranes were associated with cytoplasmic chromatin (Figure 2F, right), consistent with ER tubule invasion into disrupted MN chromatin.

To further characterize the change in chromatin structure associated with NE collapse, we analyzed the size and intensity of DAPI staining in disrupted MN. We observed that disrupted MN were frequently smaller and more condensed than intact MN (Figure S2G and S2F). Consistent with an increase in chromatin compaction, we also observed a strong correlation between MN disruption and the loss of acetyl-histone3-K9, a mark of open chromatin (Figure S2I). Taken together, these data indicate that MN disruption is caused by NE collapse, which is characterized by chromatin compaction and a failure to exclude ER tubules from the chromatin mass.

NE collapse is triggered by lamin disorganization

Research from our lab showed that NE rupturing in PN was closely associated with defects in the nuclear lamina (Vargas et al., 2012). To determine if the lamina was similarly compromised in MN prior to NE collapse, we examined the localization of lamin B1 (LmnB1) in intact MN. Two morphologies were observed: 1) a continuous nuclear rim of LmnB1, similar to the PN, and 2) discontinuous LmnB1 labeling characterized by one or more large holes in the lamina (Figure 3A). To determine if MN disruption is linked to lamina discontinuities, we monitored RFP-tagged LmnB1 in MN by time-lapse imaging. In 19/19 MN we observed large lamin discontinuities developing prior to NE collapse (Movie S5). In several cases these holes were apparent soon after NE re-formation at the end of mitosis (Movie S6). We did not observe contraction of the lamin holes in intact MN during interphase, indicating that the holes are stable and resistant to repair. These data suggest that lamina disorganization, which can occur at different stages in interphase by mechanisms that remain to be determined, triggers MN disruption.

Author Manuscript Author Manuscript Author Manuscript Author Manuscript

After disruption, LmnB1 often loses peripheral localization and appears collapsed (Figure 3A, Movie S5, S6), similar what we previously observed for the NE. Analysis of fixed cells indicated that the collapsed lamin morphology was strongly correlated with disrupted MN (Figure 3B).

Previous work has shown that loss of LmnB1 causes holes to form in the lamina (Vergnes et al., 2004) and significantly increases the frequency of NE rupturing (Vargas et al., 2012). To determine if LmnB1 levels similarly affected MN disruption, we depleted LmnB1 in U2OS cells and observed MN integrity. We observed a significant increase in the proportion of disrupted MN in LmnB1 depleted cells compared to controls (Figure 3C and S3A). This effect was not seen upon depletion of either LmnB2 or LmnA/C (Figure S3A-S3C) and was enhanced by further reducing LmnB1 levels through transfection of a LmnB1 siRNA (Figure S3D and S3E). Expression of non-degradable LmnB1 reduced MN disruption to control levels (Figure 3C, S3D, and S3E), indicating that MN disruption is a specific to LmnB1 depletion. We also analyzed LmnB1 organization in intact MN by super-resolution microscopy and found that it was characterized by large holes in the lamina similar to LmnB1-depleted PN (Figure 3D). We did not detect phosphorylated lamins in MN, indicating that lamina disruption is independent of mitotic kinase activity (data not shown). These data suggest that NE collapse in MN is linked to LmnB1 depletion specifically.

To determine whether lamin overexpression is sufficient to inhibit MN disruption, we expressed Lmn B2 in U2OS cells (Figure S3H and S3I). LmnB2 was used because it has overlapping functions with LmnB1 in maintaining nuclear structure (Coffinier et al., 2010), but, unlike LmnB1, does not cause large-scale structural alterations upon overexpression (Schumacher et al., 2006). We observed a significant increase in intact MN in cells expressing LmnB2 compared to control cells (Figure 3F). Thus, our data suggest that MN disruption results from lamina disorganization, specifically decreased LmnB1 levels, and that increasing lamin B levels can prevent disruption.

MN disruption causes broad micronuclear dysfunction

Compartmentalization is a prerequisite for proper localization and concentration of proteins in the nucleus that is the basis of regulated genome functioning. Therefore, we assessed the impact of MN disruption on nuclear functions and asked whether it could explain the defects that had been previously identified in MN. We first assessed transcription by labeling cells with an antibody to active RNAPolII, RNAPolII-phospho-S2, which is specific for elongating RNAPolII (Ni et al., 2004). We observed that RNAPolIIpS2 was present in the majority of intact MN but absent from almost all disrupted MN (Figure 4A and 4B). We also examined nuclear mRNA content by oligo-dT fluorescence *in situ* hybridization and found that mature mRNAs were present in both intact MN and PN, but absent in disrupted MN (Figure S4A). These data indicate that disruption is strongly correlated with a complete loss of transcription.

To determine the impact of MN disruption on DNA replication, we synchronized cells by mitotic shake-off and released them into interphase in the presence of EdU. After 24 h we found that in cells with EdU positive PN almost all disrupted MN completely lacked EdU labeling (Figure 4C and 4D). In contrast, the majority of intact MN incorporated EdU,

Author Manuscript Author Manuscript Author Manuscript Author Manuscript

although about 20% lacked EdU labeling. This defect in replication in intact MN is consistent with previous work demonstrating delays in early replication factor recruitment to MN (Crasta et al., 2012). However, our data indicate that MN disruption is strongly correlated with a complete arrest of DNA replication.

Finally, we asked whether DNA damage repair was impaired specifically in disrupted MN. To assess levels of DNA damage, we looked for foci of γ-H2AX, a modified histone found at sites of double-stranded DNA breaks (DSBs) (Ciccia and Elledge, 2010). We found multiple foci or a single large focus of accumulated γ-H2AX in around 60% of disrupted MN yet rarely in intact MN (Figure 4E and 4F). The appearance of γ-H2AX foci could be prevented by overexpression of lamin B2 (Figure S4B), confirming a strong correlation between MN disruption and DNA damage accumulation. We also analyzed when in the cell cycle disrupted MN accumulated DNA damage and found that the proportion of disrupted MN with γ-H2AX labeling was significantly higher in S and G2 phase compared to G1 (Figure S4C). No change was observed in intact MN (data not shown). Labeling of cells with cleaved-caspase 3 indicated that γ-H2AX positive MN were not associated with apoptotic cells (Figure S4D). Together these data indicate that DNA damage accumulation is strongly correlated with MN disruption.

The γ-H2AX signal in disrupted MN could represent either new DNA damage occurring after disruption or a failure to repair DNA damage occurring in intact MN. To discriminate between these possibilities, we treated G1 cells with doxorubicin, a DSB inducer, and quantified γ-H2AX foci. Doxorubicin caused multiple γ-H2AX foci to appear in 100% of the PN and the majority of intact MN, but foci were largely absent from disrupted MN (Figure 4G and 4H), indicating that disrupted MN can neither sense new DNA damage, nor repair existing damage.

DNA damage does not cause MN disruption

The lack of intact MN with accumulated γ-H2AX and the inability of disrupted MN to acquire DNA damage marks suggests that DNA damage and MN disruption likely occur concurrently. Previous work has shown that DNA damage can affect nuclear organization (Misteli and Soutoglou, 2009), thus we wanted to know if DNA damage could cause MN disruption. We first examined the effect of inducing DSBs on MN disruption. G1 cells, which largely contain intact MN, were treated with either DMSO or doxorubicin for 1 h. The drug was then washed out and cells were allowed to recover for 20 h. We found that, although DNA damage persisted in the doxorubicin treated nuclei for at least 20 h after release (Figure 5A), the proportion of disrupted MN was the same in cells treated with DMSO or doxorubicin (Figure 5B), indicating that DSB formation and recruitment of DNA damage repair proteins do not increase MN disruption frequency.

To confirm this finding we examined the effect of replication stress on MN disruption by incubating G1 cells with varying concentrations of HU. HU arrests cells in S-phase by causing replication fork stalling and collapse, which develop into one-sided DSBs (Petermann et al., 2010). We examined the proportion of disrupted MN after a 24 h incubation and found that, although γ-H2AX foci numbers increased in PN (Figure 5C) and intact MN (Figure 5D) with increasing concentrations of HU, there was no significant

Author Manuscript Author Manuscript Author Manuscript Author Manuscript

difference in the proportion of disrupted MN (Figure 5E). Thus, disruption appears to be the cause, not the consequence, of DNA damage accumulation in MN.

MN disruption in non-small cell lung cancer

To determine if MN disruption was limited to cultured cells, or if it occurred in solid tumors as well, we observed the localization of LSD-1, a direct marker of nuclear integrity (Figure 1D), and γ-H2AX, a marker of the loss of functionality in disrupted MN, in paraffin sections of human non-small cell lung cancer (NSCLC) tumors. NSCLC tumors are characterized by a high level of chromosomal instability (Nakamura et al., 2003; Birkbak et al., 2011), and are thus likely to have a high frequency of MN. MN were identified using two criteria: first, the chromatin mass had to be completely contained within in the paraffin section z-plane, and second the chromatin mass had to be present in the same cell as a larger PN. The latter was determined using antibodies to E-cadherin to label cell junctions. Using LSD-1 and γ-H2AX labeling, we identified two populations of MN in NSCLC tumors. The first had high levels of LSD-1 and no γ-H2AX labeling, indicative of an intact MN (Figure 6A, top). The second had no LSD-1 labeling and high levels of γ-H2AX, indicative of disrupted MN that had accumulated DNA damage (Figure 6A, bottom). Further examination of the γ-H2AX positive MN showed that they also lacked TPR and acetyl-histone3K9 (Figure S5A and S5B), and were present in non-apoptotic cells (Figure S5C), indicating that they represent true disrupted MN.

Disrupted MN were identified in 2/3 pulmonary adenocarcinomas and 1/1 squamous cell carcinomas. The presence of disrupted MN in tumor cells of both types was confirmed by pseudo-coloring DAPI and Sypro Ruby staining to resemble hematoxylin and eosin staining, respectively (Figure 6B and 6C). Taken together, these data indicate that MN disruption occurs *in vivo* in solid tumors.

Discussion

Historically MN have been considered passive indicators of chromosomal instability. A growing body of evidence has shown, however, that being segregated into an MN has important negative consequences for the chromatin that could drive chromosomal instability (Hoffelder et al., 2004; Terradas et al., 2009, 2012; Xu et al., 2011; Crasta et al., 2012). In the present study we demonstrate that synchronized broad MN dysfunction and massive DNA damage result from irreversible NE collapse in MN in both cultured cells and solid tumors. We found that during interphase most MN in a population of cells lose compartmentalization after irreversible NE collapse. Loss of NE integrity arrests basic nuclear functions including replication, transcription, and DNA damage recognition and repair. NE collapse in MN is preceded by defects in lamin organization specifically linked to decreased levels of lamin B1. Disrupted MN are characterized by large conformation changes in the chromatin and associated ER membranes and INM proteins, which likely inhibit NE repair (Figure 6D). Importantly, disrupted MN were identified not only in cultured cancer cells, but also in human tumors, immortalized epithelial cells, and primary fibroblasts. Thus, NE collapse and subsequent disruption of MN functioning appears to be a general consequence of MN formation.

Author Manuscript Author Manuscript Author Manuscript Author Manuscript

Mechanism of MN disruption

Our data reveal a previously undetected structural defect in the lamina of MN that destabilizes the NE. However, it is unclear what causes discontinuities to form specifically in the MN lamina. Our imaging of LmnB1 in MN after mitosis provides evidence that holes can be present almost concurrently with NE formation. This timing is consistent with a defect in NE formation, rather than a failure to maintain or import lamin-associated proteins in interphase, although the latter could contribute to hole growth. NE formation is a highly orchestrated multi-step process and lamina assembly is one of the last steps (Burke and Ellenberg, 2002). Thus, any problems early in NE assembly could have downstream effects on lamina disorganization. Identifying the mechanism underlying lamina disorganization in MN could thus provide important information about how NE formation is regulated.

NE collapse in MN differs from that in PN in that it is usually irreparable. At this time almost nothing is known about how the NE repairs itself in PN, but the mechanism would have to result in re-spreading of the ER/NE membrane over the chromatin. There are two possible sources of this membrane, one is the existing NE, and the second is ER tubules or sheets interacting with the chromatin and subsequently forming an NE, similar to what occurs during NE formation (Anderson and Hetzer, 2008b). Our data indicate that ER tubules do contact the exposed chromatin, but fail to reform an intact NE. Concurrent with NE collapse we also observed significant chromatin compaction. Although our data does not indicate which event occurs first or if NE collapse and chromatin compaction are mechanistically linked, one possibility is that chromatin condensation prevents either NE repair or new NE formation. This model is consistent with the idea that NE formation during mitotic exit, in addition to the orchestrated action of cell cycle-specific phosphatase (Ramadan et al., 2007), requires chromosome decondensation to recruit INM protein to the chromatin surface (Hetzer, 2010). Thus, understanding why disrupted MN have aberrant connections with ER tubules in interphase could provide important insights into both NE formation and interphase NE repair.

Consequences of MN disruption

Our data demonstrate that MN disruption results in a global cessation of nuclear functions. However, our data and that of previous studies demonstrate that there are defects in intact MN functioning as well, specifically in recruitment of DNA repair and replication proteins (Crasta et al., 2012; Terradas et al., 2012). Previously, MN were thought to be structurally similar to PN, but our study identifies a severe problem with lamina organization in MN. This disorganization may not only prime MN for NE collapse but also impair functioning in intact MN as disrupting the lamin B1 network in PN has been shown to impair both transcription (Spann et al., 2002; Tang et al., 2008) and DNA replication (Spann et al., 1997).

Our work indicates that the time of DNA damage accumulation, specifically γ-H2AX accumulation, is restricted to when disruption occurs. However, our data are consistent with a model where the accumulation of DNA damage is context dependent. Previous work has suggested that DNA damage in MN is the result of incomplete DNA replication (Xu et al., 2011; Crasta et al., 2012). In our study we observed a significant increase in γ-H2AX

Author Manuscript Author Manuscript Author Manuscript Author Manuscript

positive MN specifically in S and G2 phases as well as intact MN with impaired DNA replication (see Figure 4D). These data are consistent with a model where DNA replication sensitizes intact MN to DNA damage, which is triggered by MN disruption. Although we did not observe a significant impairment of NPC assembly or active accumulation of nuclear proteins in intact MN, in contrast to previous reports (Hoffelder et al., 2004; Terradas et al., 2009; Crasta et al., 2012), this does not rule out defective transport of specific proteins important for processes like DNA replication into intact MN. It will be of great interest to determine the mechanism of DNA damage in MN and how disruption can induce a massive accumulation of fragmented DNA that could drive chromothripsis (Crasta et al., 2012).

In principle, the arrest of transcription and DNA replication and the induction of DNA damage can all promote aneuploidy. Loss of transcription can generate a temporary aneuploidy in interphase cells and if the segregated chromatin contains important regulators for processes like genomic stability, this could be sufficient to induce more permanent genomic alterations. The loss of DNA replication causes the cell to enter mitosis as 2n-1, guaranteeing that one daughter cell will be aneuploid. Finally, previous work has shown that DNA damage in MN results in extensive DNA fragmentation in both interphase and mitosis (Terradas et al., 2009; Crasta et al., 2012). These chromatin pieces are hypothesized to be source material for the massive single-chromosome rearrangement process termed chromothripsis (Crasta et al., 2012), which occurs in a wide variety of cancers (Stephens et al., 2011). Our work refines this model by demonstrating a strong correlation between NE collapse in MN and the accumulation of DNA damage.

MN disruption and cancer

Chromothripsis strongly correlates with poor prognosis in cancer patients (Rausch et al., 2012) and is postulated to occur early in carcinogenesis (Forment et al., 2012). For disrupted MN to play a significant role early in carcinogenesis, they should occur in healthy cells. Although MN frequency is low in normal cells, estimates suggest 0.5 to 2.5 MN occur per 1000 human buccal cells (Holland et al., 2008), we did observe MN disruption occurring in non-transformed cell lines, consistent with previous reports of γ-H2AX positive MN in these types of cells (Terradas et al., 2009; Xu et al., 2011; Crasta et al., 2012). Thus MN disruption could be an important early event in cancer development.

At this time there are few objective markers for genomic instability in solid tumors, although diagnosis of several cancers relies on the identification of aneuploidy. MN have been used extensively to identify genomic instability in peripheral blood cells or epithelial cell scrapings (Holland et al., 2008), but are hard to positively identify in tumor sections. Our ability to identify disrupted MN in solid tumors suggests a new way to evaluate aneuploidy in these tissues. Disrupted MN are readily identifiable in 5 μm thick NSCLC sections by fluorescent microscopy even at low magnification due to their characteristic accumulation of γ-H2AX (see Figure 6C). This is in contrast to intact MN, which require analysis of the entire z projection and can be difficult to distinguish from cut-off PN. Our analysis in tissue culture cells suggests that disrupted MN represent a high and regular percentage of the total population of MN in an asynchronous fixed sample. It will be of great interest to examine

Author Manuscript Author Manuscript Author Manuscript Author Manuscript

how MN disruption frequency compares to standard and more time-consuming assays for aneuploidy in solid tumors and whether it represents a new diagnostic structural trait.

Our findings suggest that NE collapse in MN is the result of decreased lamin B1 and subsequent disruption of the lamina. This collapse results in lasting MN damage that can affect genomic stability. It remains unclear why this event is specific to MN and why similar events do not seem to occur during developmental karyomere formation. Further analysis promises to be informative about both the mechanism of NE repair in interphase and NE formation after mitosis. In addition, our data indicate a new connection between aberrant NE dynamics and carcinogenesis that may prove to be a valuable tool for cancer diagnosis.

Experimental Procedures

Cell culture and transfection

U2OS, DU145, HeLa, and MDA-MB-231 cells were grown in DMEM + 10% FBS at 10% CO_2. hTERT-RPE-1 cells were grown in DMEM/F12 + 10% FBS + 0.01 mg/mL hygromycin at 5% CO_2. IMR90 cells were grown in DMEM with Glutamax (Gibco) + 15% FBS + non-essential amino acids (Gibco) at 7.5% CO_2, 3% O_2. Plasmids were transfected using Lipofectamine 2000 and siRNAs were transfected using RNAimax according to manufacturer's instructions (both Life Technologies). Cells were analyzed at least 2 d post transfection. Details on the stable cell lines, plasmids, and siRNAs used in this study are in the extended experimental procedures.

For mitotic shake-off experiments, cells were incubated in 100 ng/mL nocodazole for up to 6 h prior to synchronization by shake-off onto coverslips in fresh medium. EdU was added to the medium at 10 μm for pulse-labeling and 5 μm for long-term labeling experiments. Hydroxyurea was used at 2 mM and RO-3306 (Enzo) was used at 10 μm. Doxorubicin was used at 5 μm to assess DNA damage in disrupted MN and at 0.5 μm to asses MN disruption after DNA damage. Leptomycin B was used at 0.1 mg/mL. For time-lapse imaging, cells were incubated in 0.1 μg/mL Hoechst for 15 m at 37°C and fresh medium added prior to imaging.

Immunofluorescence and FISH

Antibodies used for immunofluorescence are listed in the extended experimental procedures. For indirect immunofluorescence cells were grown on coverslips and fixed in 4% PFA in 1× PBS for 10 min at RT. Coverslips were blocked in 3% BSA in PBS + 0.1% TritonX-100 prior to incubation in primary and secondary antibodies diluted in blocking buffer. Coverslips were briefly incubated with DAPI (1 μg/mL in PBS; Roche) and mounted in Vectashield (Vector Labs). For structured illumination microscopy (SIM) analysis, cells were grown on Zeiss high-performance coverslips and mounted in ProLong Gold (Life Technologies).

Human non-small cell carcinoma resection specimens were fixed in normal buffered formalin for 12-72 h before standard histologic paraffinization (Fischer et al., 2008). Five μm sections were cut from the paraffinized blocks of tissue and mounted on Fisher Plus microscope slides. Paraffin sections were rehydrated in xylene and a graduated ethanol

Author Manuscript Author Manuscript Author Manuscript Author Manuscript

series. Antigen retrieval was performed by boiling in 0.01 M citric acid pH 6 for 15 m. Slides were blocked in 3% BSA and 4% goat serum in 1×PBS + 0.1% TritonX-100 prior to incubation in antibody dilutions and DAPI. If necessary, slides were incubated in Sypro Ruby (Life Technologies) overnight at 4°C prior to DAPI staining. Sections were mounted in ProLong Gold.

For fluorescent *in situ* hybridization, cells grown on coverslips were fixed for 10 m RT in 4% PFA, and processed for *in situ* hybridization using a previously described protocol (http://www.singerlab.org/protocols). Cells were incubated in 0.3 ng/μL Alexa-568-polydT(50) probe (custom ordered; Life Technologies) overnight at 37°C. Indirect immunofluorescence was then performed as described above.

Fixed samples were imaged on a Zeiss LSM 710 scanning confocal microscope with a 63× 1.4NA oil immersion or a 20× 0.8NA air objective with Zen software (Zeiss). Images are single confocal sections except where noted. Images were adjusted for brightness and contrast using ImageJ (Abràmoff et al., 2004) or Photoshop CS3 (Adobe). All Z-stacks were taken at 0.5 μm intervals. SIM was performed using a Zeiss Elyra PS.1 Super-Resolution microscope with a 63× 1.4NA oil immersion objective. Images were acquired and processed with Zen 2012 software (Zeiss).

TEM

Cells were grown on MatTek 35 mm petri dishes with a 14 mm microwell, fixed in 2% glutaraldehyde in 0.1 M Na cacodylate buffer, pH 7.3, washed, and incubated in 1% osmium tetroxide followed by 2% uranyl acetate. After embedding in Durcupan (Electron Microscopy Sciences) thin sections (70 nm) were cut on an ultramicrotome (Leica) and post-stained with 2% uranyl acetate and Sato's Lead stain. Sections were examined on a JEOL 1200ex TEM, and images were captured on film.

Time-lapse imaging

Cells were plated into 8-well μ-slide chambers (iBidi) and imaged on a Zeiss Axioscope/ Yokagawa spinning disk confocal microscope with a 63× 1.4NA oil objective or a 20× 0.8 NA air objective at 37°C and 10% CO_2. Images were captured with an EM CCD camera (Hamamatsu) using AxioVision software (Zeiss). Videos were cropped and adjusted for brightness and contrast using ImageJ and Photoshop.

Quantification of images and western blots

Western blot bands were quantified using a fluorescent imager (Odyssey; Li-Cor) and ImageJ. The integrated density of the bands was background subtracted and normalized to GAPDH prior to comparison. Prism5 (GraphPad) was used to generate all graphs and perform statistical analyses. Detailed explanation of fluorescence intensity quantification and statistics are in the extended experimental procedures.

Supplementary Material

Refer to Web version on PubMed Central for supplementary material.

Author Manuscript Author Manuscript Author Manuscript Author Manuscript

Acknowledgements

We would like to thank Jamie Kasuboski in the Waitt Advanced Biophotonics Core at the Salk Institute for performing structured illumination microscopy and members of the Hetzer lab for critical comments. M.W.H, is supported by the National Institutes of Health grant R01GM098497 and a scholar award from the American Cancer Society. E.H. is supported by a Postdoctoral Fellowship, PF-12-137-01-CSM, from the American Cancer Society. The project described was supported by Award Number P30CA014195 from the National Cancer Institute.

References

Abràmoff MD, Hospitals I, Magalhães PJ, Abràmoff M. Image Processing with ImageJ. Biophotonics International. 2004; 11:36–42.

Anderson DJ, Hetzer MW. Nuclear envelope formation by chromatin-mediated reorganization of the endoplasmic reticulum. Nat Cell Biol. 2007; 9:1160–1166. [PubMed: 17828249]

Anderson DJ, Hetzer MW. Reshaping of the endoplasmic reticulum limits the rate for nuclear envelope formation. J Cell Biol. 2008a; 182:911–924. [PubMed: 18779370]

Anderson DJ, Hetzer MW. Shaping the endoplasmic reticulum into the nuclear envelope. J Cell Sci. 2008b; 121:137–142. [PubMed: 18187447]

Birkbak NJ, Eklund AC, Li Q, McClelland SE, Endesfelder D, Tan P, Tan IB, Richardson AL, Szallasi Z, Swanton C. Paradoxical relationship between chromosomal instability and survival outcome in cancer. Cancer Research. 2011; 71:3447–3452. [PubMed: 21270108]

Burke B, Ellenberg J. Remodelling the walls of the nucleus. Nature Reviews Molecular Cell Biology. 2002; 3:487–497.

Ciccia A, Elledge SJ. The DNA damage response: making it safe to play with knives. Molecular Cell. 2010; 40:179–204. [PubMed: 20965415]

Cimini D, Howell B, Maddox P, Khodjakov A, Degrassi F, Salmon ED. Merotelic kinetochore orientation is a major mechanism of aneuploidy in mitotic mammalian tissue cells. The Journal of Cell Biology. 2001; 153:517–527. [PubMed: 11331303]

Coffinier C, Chang SY, Nobumori C, Tu Y, Farber EA, Toth JI, Fong LG, Young SG. Abnormal development of the cerebral cortex and cerebellum in the setting of lamin B2 deficiency. Proc Natl Acad Sci U S A. 2010; 107:5076–5081. [PubMed: 20145110]

Crasta K, Ganem NJ, Dagher R, Lantermann AB, Ivanova EV, Pan Y, Nezi L, Protopopov A, Chowdhury D, Pellman D. DNA breaks and chromosome pulverization from errors in mitosis. Nature. 2012; 482:53–58. [PubMed: 22258507]

Fenech M. Cytokinesis-block micronucleus cytome assay. Nat Protoc. 2007; 2:1084–1104. [PubMed: 17546000]

Fischer AH, Jacobson KA, Rose J, Zeller R. Paraffin Embedding Tissue Samples for Sectioning. Cold Spring Harbor Protocols. 2008; 2008 pdb.prot4989-pdb.prot4989.

Forment JV, Kaidi A, Jackson SP. Chromothripsis and cancer: causes and consequences of chromosome shattering. Nature Reviews. Cancer. 2012; 12:663–670.

Frosst P, Guan T, Subauste C, Hahn K, Gerace L. Tpr is localized within the nuclear basket of the pore complex and has a role in nuclear protein export. The Journal of Cell Biology. 2002; 156:617–630. [PubMed: 11839768]

Gant TM, Wilson KL. Nuclear assembly. Annual Review of Cell and Developmental Biology. 1997; 13:669–695.

Hetzer MW. The nuclear envelope. Cold Spring Harb Perspect Biol. 2010; 2:a000539. [PubMed: 20300205]

Hoffelder DR, Luo L, Burke NA, Watkins SC, Gollin SM, Saunders WS. Resolution of anaphase bridges in cancer cells. Chromosoma. 2004; 112:389–397. [PubMed: 15156327]

Holland N, Bolognesi C, Kirsch-Volders M, Bonassi S, Zeiger E, Knasmueller S, Fenech M. The micronucleus assay in human buccal cells as a tool for biomonitoring DNA damage: the HUMN project perspective on current status and knowledge gaps. Mutation Research. 2008; 659:93–108. [PubMed: 18514568]

Author Manuscript Author Manuscript Author Manuscript Author Manuscript

Kim Y, Sharov AA, McDole K, Cheng M, Hao H, Fan C-M, Gaiano N, Ko MSH, Zheng Y. Mouse B-type lamins are required for proper organogenesis but not by embryonic stem cells. Science (New York, N.Y.). 2011; 334:1706–1710.

Lemaitre J-M. Dynamics of the Genome during Early Xenopus laevis Development: Karyomeres As Independent Units of Replication. The Journal of Cell Biology. 1998; 142:1159–1166. [PubMed: 9732278]

Li M, Fang X, Baker DJ, Guo L, Gao X, Wei Z, Han S, Van Deursen JM, Zhang P. The ATM-p53 pathway suppresses aneuploidy-induced tumorigenesis. Proceedings of the National Academy of Sciences of the United States of America. 2010; 107:14188–14193. [PubMed: 20663956]

Lu L, Ladinsky MS, Kirchhausen T. Formation of the postmitotic nuclear envelope from extended ER cisternae precedes nuclear pore assembly. The Journal of Cell Biology. 2011; 194:425–440. [PubMed: 21825076]

Mackay DR, Elgort SW, Ullman KS. The nucleoporin Nup153 has separable roles in both early mitotic progression and the resolution of mitosis. Molecular Biology of the Cell. 2009; 20:1652–1660. [PubMed: 19158386]

Misteli T, Soutoglou E. The emerging role of nuclear architecture in DNA repair and genome maintenance. Nature Reviews. Molecular Cell Biology. 2009; 10:243–254.

Nakamura H, Saji H, Idiris A, Kawasaki N, Hosaka M, Ogata A, Saijo T, Kato H. Chromosomal Instability Detected by Fluorescence in Situ Hybridization in Surgical Specimens of Non-Small Cell Lung Cancer Is Associated with Poor Survival. Clin. Cancer Res. 2003; 9:2294–2299. [PubMed: 12796398]

Ni Z, Schwartz BE, Werner J, Suarez J-R, Lis JT. Coordination of Transcription, RNA Processing, and Surveillance by P-TEFb Kinase on Heat Shock Genes. Molecular Cell. 2004; 13:55–65. [PubMed: 14731394]

Paulin-Levasseur M, Blake DL, Julien M, Rouleau L. The MAN antigens are non-lamin constituents of the nuclear lamina in vertebrate cells. Chromosoma. 1996; 104:367–379. [PubMed: 8575249]

Petermann E, Orta ML, Issaeva N, Schultz N, Helleday T. Hydroxyurea-stalled replication forks become progressively inactivated and require two different RAD51-mediated pathways for restart and repair. Molecular Cell. 2010; 37:492–502. [PubMed: 20188668]

Ramadan K, Bruderer R, Spiga FM, Popp O, Baur T, Gotta M, Meyer HH. Cdc48/p97 promotes reformation of the nucleus by extracting the kinase Aurora B from chromatin. Nature. 2007; 450:1258–U13. [PubMed: 18097415]

Rausch T, Jones DTW, Zapatka M, Stütz AM, Zichner T, Weischenfeldt J, Jäger N, Remke M, Shih D, Northcott PA, et al. Genome sequencing of pediatric medulloblastoma links catastrophic DNA rearrangements with TP53 mutations. Cell. 2012; 148:59–71. [PubMed: 22265402]

Schumacher J, Reichenzeller M, Kempf T, Schnolzer M, Herrmann H. Identification of a novel, highly variable amino-terminal amino acid sequence element in the nuclear intermediate filament protein lamin B(2) from higher vertebrates. FEBS Lett. 2006; 580:6211–6216. [PubMed: 17070523]

Spann TP, Goldman AE, Wang C, Huang S, Goldman RD. Alteration of nuclear lamin organization inhibits RNA polymerase II-dependent transcription. J Cell Biol. 2002; 156:603–608. [PubMed: 11854306]

Spann TP, Moir RD, Goldman AE, Stick R, Goldman RD. Disruption of nuclear lamin organization alters the distribution of replication factors and inhibits DNA synthesis. The Journal of Cell Biology. 1997; 136:1201–1212. [PubMed: 9087437]

Stephens PJ, Greenman CD, Fu B, Yang F, Bignell GR, Mudie LJ, Pleasance ED, Lau KW, Beare D, Stebbings LA, et al. Massive genomic rearrangement acquired in a single catastrophic event during cancer development. Cell. 2011; 144:27–40. [PubMed: 21215367]

Tang CW, Maya-Mendoza A, Martin C, Zeng K, Chen S, Feret D, Wilson SA, Jackson DA. The integrity of a lamin-B1-dependent nucleoskeleton is a fundamental determinant of RNA synthesis in human cells. J Cell Sci. 2008; 121:1014–1024. [PubMed: 18334554]

Terradas M, Martín M, Hernández L, Tusell L, Genescà A. Nuclear envelope defects impede a proper response to micronuclear DNA lesions. Mutation Research. 2012; 729:35–40. [PubMed: 21945242]

Author Manuscript Author Manuscript Author Manuscript Author Manuscript

Terradas M, Martín M, Tusell L, Genescà A. DNA lesions sequestered in micronuclei induce a local defective-damage response. DNA Repair. 2009; 8:1225–1234. [PubMed: 19683478]

Thompson SL, Compton DA. Chromosome missegregation in human cells arises through specific types of kinetochore-microtubule attachment errors. Proceedings of the National Academy of Sciences of the United States of America. 2011; 108:17974–17978. [PubMed: 21997207]

Vargas JD, Hatch EM, Anderson DJ, Hetzer MW. Transient nuclear envelope rupturing during interphase in human cancer cells. Nucleus. 2012; 3:88–100. [PubMed: 22567193]

Vergnes L, Peterfy M, Bergo MO, Young SG, Reue K. Lamin B1 is required for mouse development and nuclear integrity. Proc Natl Acad Sci U S A. 2004; 101:10428–10433. [PubMed: 15232008]

Voeltz GK, Prinz WA, Shibata Y, Rist JM, Rapoport TA. A class of membrane proteins shaping the tubular endoplasmic reticulum. Cell. 2006; 124:573–586. [PubMed: 16469703]

Xu B, Sun Z, Liu Z, Guo H, Liu Q, Jiang H, Zou Y, Gong Y, Tischfield JA, Shao C. Replication stress induces micronuclei comprising of aggregated DNA double-strand breaks. PloS One. 2011; 6:e18618. [PubMed: 21525980]

Author Manuscript Author Manuscript Author Manuscript Author Manuscript

Highlights

- Micronuclei frequently undergo irreversible nuclear envelope collapse
- Lamin B1 levels influence the likelihood of nuclear envelope collapse
- Massive DNA damage accumulation in micronuclei occurs upon collapse
- Micronuclei disruption occurs in solid tumors as well as normal and cancer cells

Author Manuscript Author Manuscript Author Manuscript Author Manuscript

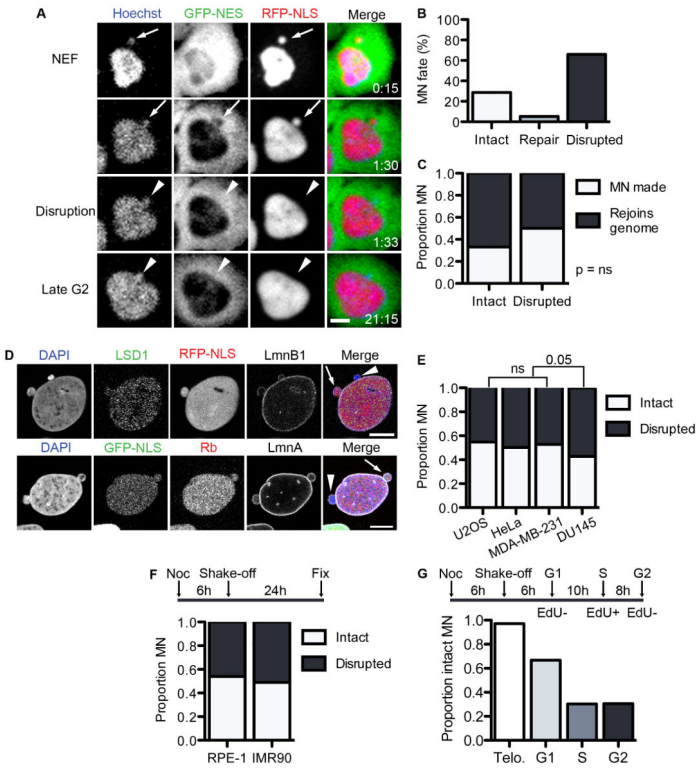

Figure 1. Micronuclei frequently and irreversibly lose compartmentalization in interphase cells

(A) Stills from time-lapse imaging of U2OS 2×RFP-NLS (RFP-NLS) cells expressing 4×GFP-NES (GFP-NES) and labeled with Hoechst. NEF = NE formation. Time is h:m. Scale bar = 10 μm. (B) Quantification of MN fate during interphase from time-lapse imaging. N = 122 MN from 3 experiments. (C) Quantification of MN fate after mitosis from time-lapse imaging of U2OS GFP-IBB mCherry-H2B cells. N = 44 intact MN and 165 disrupted MN from 3 experiments. $P > 0.05$ by Fisher's exact test, used for all data in figure. (D) Images of intact (arrows) and disrupted (arrowheads) MN in fixed U2OS cells labeled with antibodies to LSD-1 and lamin B1 (LmnB1) (top) or retinoblastoma (Rb) and lamin A (LmnA) (bottom). Scale bars = 10 μm. (E) Quantification of MN integrity and soluble nuclear protein labeling. N = 300 MN/label from 3 experiments. ϕ = Phi correlation coefficient. (F) Quantification of MN integrity in asynchronous cancer cell lines stably expressing GFP-NLS. N = 250 MN/cell line from 3 experiments. (G) Experiment schematic and quantification of MN integrity in non-transformed cell lines 24 h post mitosis. N = 300 MN/cell line from 3 experiments. (H) Experiment schematic (top) and proportion intact MN in U2OS GFP-NLS cells fixed at indicated cell cycle phase. Telophase (telo.) data are from time-lapse imaging analysis. N = 125 MN for telo. and 300 MN/time point from 3 experiments. See also Figure S1 and Movie S1.

Author Manuscript Author Manuscript Author Manuscript Author Manuscript

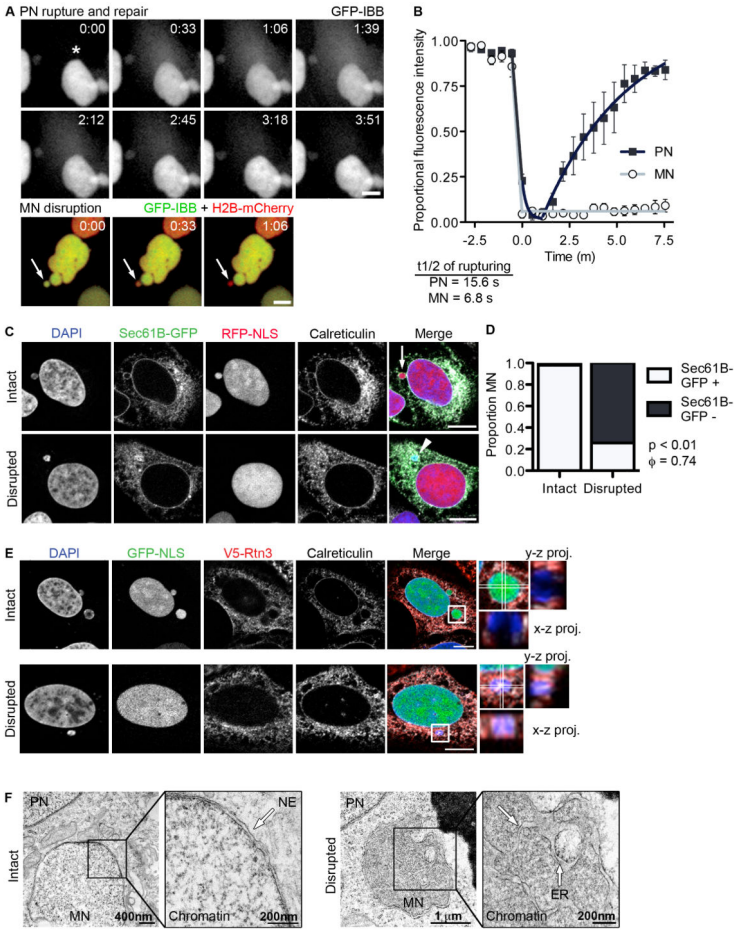

Figure 2. MN disruption occurs by NE collapse and is characterized by ER tubule invasion of the chromatin

(A) Stills from time-lapse imaging of U2OS GFP-IBB, H2B-mCherry cells undergoing PN rupturing and repair (top) and MN disruption (bottom). An asterisk indicates the site of PN NE rupturing (top) and an arrow indicates the MN (bottom). Time is m:s. All scale bars in figure = 10 μm. (B) Analysis of GFP-IBB fractional fluorescence intensity in nucleus during PN NE rupturing and MN disruption. The rupturing half-time, mean, and s.e.m are shown on graph. N = 5. (C) Images of intact and disrupted MN in U2OS RFP-NLS cells expressing Sec61B-GFP and labeled for the luminal ER protein calreticulin. (D) Quantification of Sec61B-GFP presence at the nuclear rim in intact and disrupted MN, as defined by DAPI staining. N = 300 MN/category from 3 experiments. ϕ = Phi correlation co-efficient. (E) Images of intact and disrupted MN in U2OS GFP-NLS cells expressing V5-tagged reticulon 3 (V5-Rtn3) and labeled for calreticulin. X-z and y-z projections of boxed regions cover 5.48 μm (top) and 5.97 μm (bottom) stacks, respectively. In top (intact MN) projections, GFP-NLS is omitted for clarity. (F) TEM images of intact (left) and disrupted (right) MN in U2OS GFP-NLS cells 8 h and 18 h post-mitotic shake-off, respectively. In the intact MN membranes (arrows) are excluded from the chromatin and in the disrupted MN ER membranes are visible inside the chromatin. See also Figure S2, Movie S2, Movie S3, and Movie S4.

Author Manuscript Author Manuscript Author Manuscript Author Manuscript

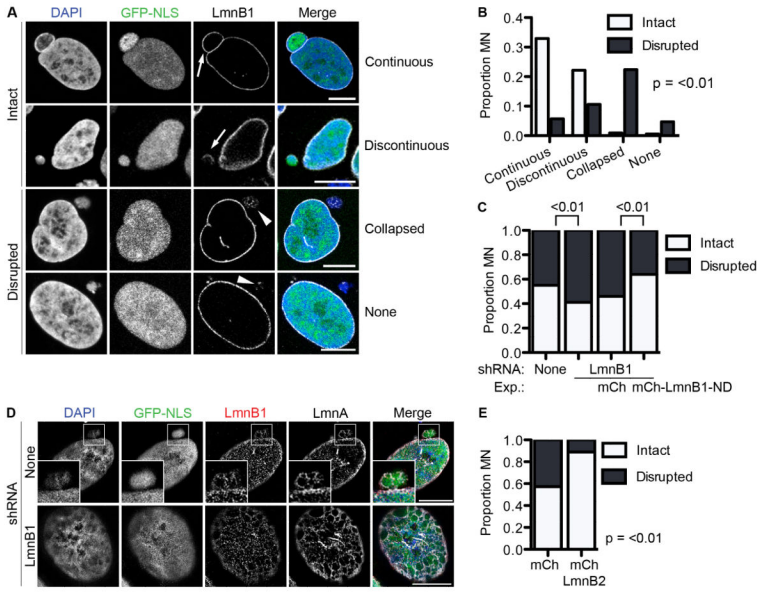

Figure 3. Depletion of lamin B1 in intact MN triggers MN disruption

(A) Images of lamin B1 (LmnB1) morphologies in intact (arrows) and disrupted (arrowheads) MN in fixed U2OS GFP-NLS cells. All scale bars in figure = 10 μm. (B) Quantification of LmnB1 morphology in asynchronous cells. N = 300 MN/category from 3 experiments. All p-values are from Fisher's exact test. (C) Quantification of MN integrity in asynchronous cell lines expressing indicated lamin B1 constructs. mCh = mCherry. ND = non-degradable. Numbers over graph represent p-values for indicated samples. N = 300 MN/cell line from 3 experiments. (D) Structured illumination images of an intact MN with a discontinuous lamina in a non-LmnB1 depleted U2OS cell (top) and the PN of a U2OS cell expressing LmnB1 shRNA (bottom) labeled with indicated antibodies. (E) Quantification of MN integrity in cell lines expressing mCherry or mCherry-LmnB2. N = 300 MN/cell line from 3 experiments. See also Figure S3, Movie S5, and Movie S6.

Author Manuscript Author Manuscript Author Manuscript Author Manuscript

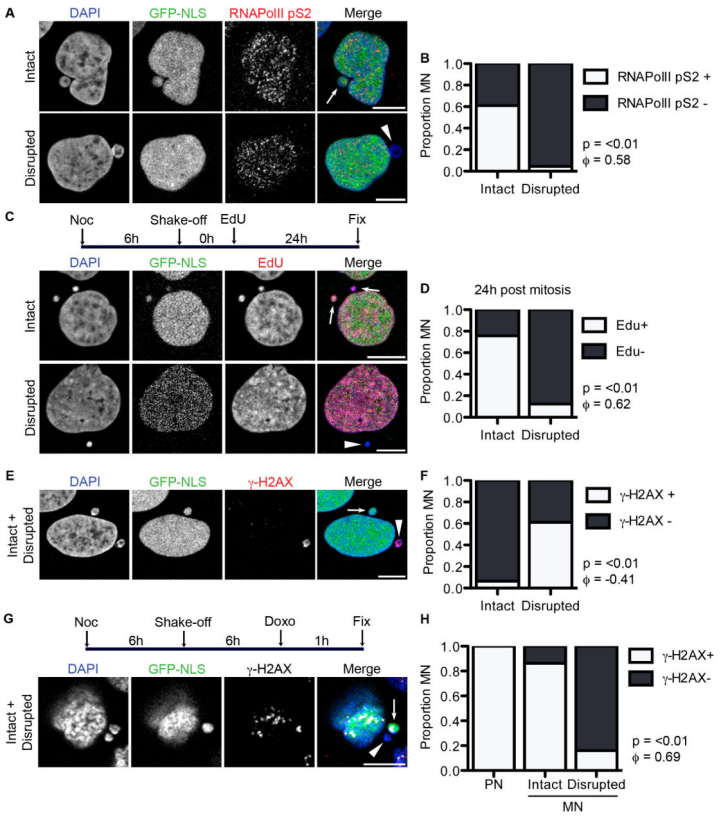

Figure 4. MN disruption causes loss of mRNA transcription, DNA replication, and DNA damage repair and sensing

(A) Images of asynchronous U2OS GFP-NLS cells fixed and labeled with the active RNA polymerase mark anti-RNAPolIIpS2. Intact and disrupted MN are indicated by arrows and arrowheads, respectively, throughout this figure. All scale bars = 10 μm. (B) Quantification of MN integrity and RNAPolIIpS2 labeling. For all quantifications in this figure, n = 300 MN/category from 3 experiments. P-value is from Fisher's exact test and ϕ = correlation co-efficient for all graphs in figure. (C) Experiment schematic and images of MN labeled with EdU for 24 h post-mitosis. (D) Quantification of MN integrity and EdU labeling in cells with EdU positive PN. (E) Image of MN labeled with anti-γ-H2AX antibody, which marks DSBs, in asynchronous cells. (F) Quantification of MN integrity and γ-H2AX labeling. (G) Experiment schematic and image of G1 cells treated with doxorubicin (doxo) for 1 h and labeled with anti-γ-H2AX. (H) Proportion of PN and intact and disrupted MN that contain more than one γ-H2AX focus or an enlarged γ-H2AX focus after 1 h doxo incubation. P and ϕ values compare only the intact and disrupted MN. See also Figure S4.

Author Manuscript Author Manuscript Author Manuscript Author Manuscript

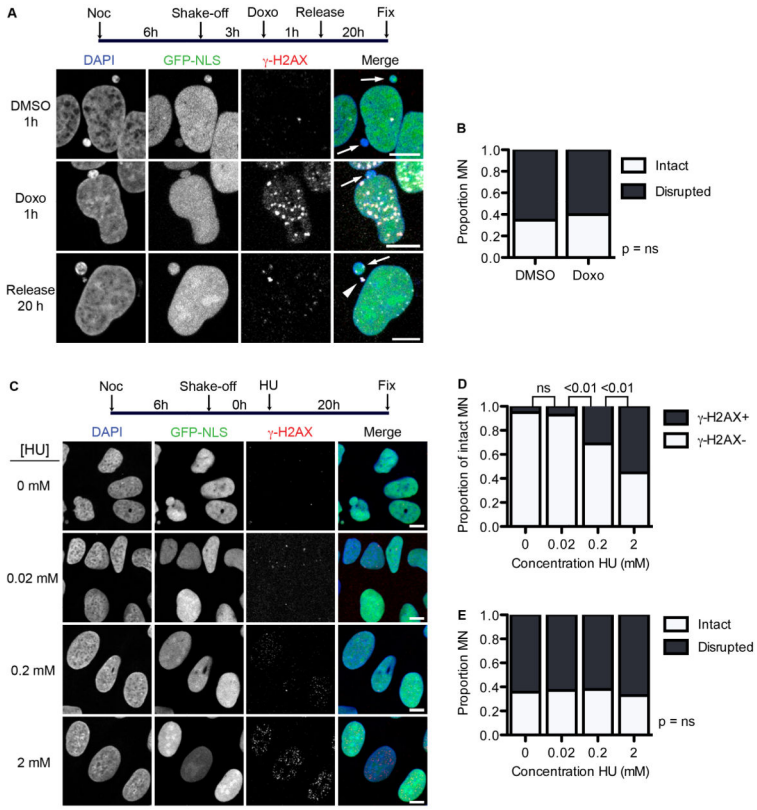

Figure 5. DNA damage does not induce MN disruption

(A) Experiment schematic and images of U2OS cells labeled with anti-γ-H2AX 20 h after 1 h incubation in DMSO or doxorubicin (doxo). All scale bars = 10 μm. Arrows and arrowheads indicate intact and disrupted MN, respectively. (B) Quantification of MN integrity in cells treated as in (A). P-value > 0.05, determined by Fisher's exact test. N = 300 MN/condition from 3 experiments. (C) Experiment schematic and images of synchronized cells treated with HU at the indicated concentrations for 20 h, fixed, and labeled with antibodies to γ-H2AX. (D) Quantification of intact MN with multiple γ-H2AX foci 20 h after HU incubation. P-values above graph refer to indicated samples determined by Fisher's exact test. N = 250 MN/concentration from 3 experiments. (E) Quantification of MN integrity in cells incubated in HU for 20 h. N = 250 MN/concentration from 3 experiments. P-value > 0.05 by χ^2 analysis.

Author Manuscript Author Manuscript Author Manuscript Author Manuscript

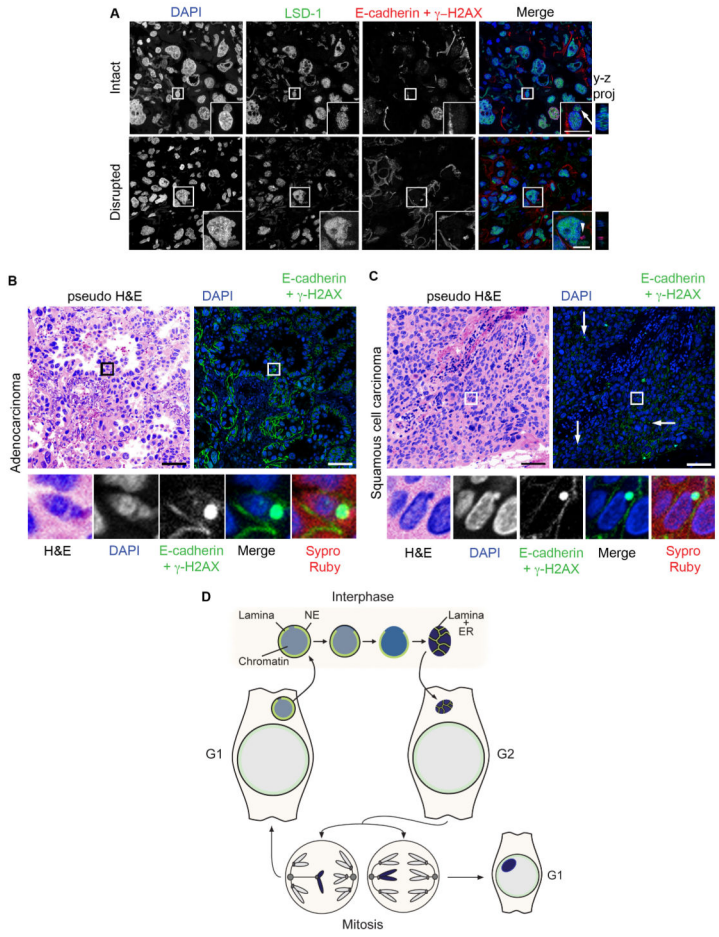

Figure 6. Disrupted MN are present in non-small cell lung cancer tumors

(A) Immunofluorescence of thin paraffin sections of a non-small cell lung cancer (NSCLC) tumor showing intact (arrow) and disrupted (arrowhead) MN. Sections were labeled with antibodies to E-cadherin, γ-H2AX, and LSD-1. Scale bars = 10 μm. Images are maximum intensity projections of 4 μm (top) and 5.5 μm (bottom) z-stacks. (B and C) Immunofluorescence of adenocarcinoma and squamous cell carcinoma tumors. Sections were labeled with antibodies to E-cadherin and γ-H2AX and stained with DAPI and Sypro Ruby. Lower panels are enlarged images of boxed area. Pseduo-hematoxylin and eosin staining (H&E) images were generated by pseudo-coloring merged DAPI/Sypro Ruby images. Arrows in (C) indicate additional disrupted MN. Scale bars = 50 μm. (D) Model of MN disruption. A lagging chromosome forms a MN upon mitotic exit. The NE of the MN may already be abnormal at this time. At some point during interphase, lamina disorganization triggers NE collapse and loss of proteins from the MN. After NE collapse, the MN chromatin becomes compacted and permeated by tubular ER. This chromatin either segregates normally or becomes a MN again in the next mitosis. See also Figure S5.